



Cite this: *CrystEngComm*, 2021, 23, 5498

Facile synthesis of ultralong hydroxyapatite nanowires using wormlike micelles as soft templates†

Junhua Zhao,^a *^a Qin Hu,^b Yinlin Lei,^{*a} Chuanhua Gao,^a Pinjie Zhang,^c Bo Zhou,^d Gongjun Zhang,^e Weijie Song,^e Xiaoge Lou^a and Xiaoli Zhou^a

As a powerful self-assembly process, the soft-template method has attracted considerable scientific interest, but there is a challenge associated with ultralong hydroxyapatite nanowires (HAPNWs) with length of tens of micrometers. In this study, we report a novel three-phase oleic acid–ethanol–water reaction system for synthesizing ultralong HAPNWs by formation of an entangled long wormlike micelle (WLM) structure. The influence of raw materials and initial pH on the HAPNW structure has been studied. Findings showed that a HAPNW structure could only be formed with a design based on the WLM structure at pH 6.5 with oleic acid or sodium oleate as a reactant. The formation mechanism of HAPNWs was proposed and analyzed. A HAPNWs/carbon composite adsorbent was used for the removal of methyl orange from the aqueous phase, showing unique adsorption properties over broad pH and temperature range from 3 to 7 and 20 to 60 °C, even though solid content of HAPNWs in composite adsorbent is only 0.038%. This fundamental research will enrich the knowledge base for controlled synthesis and applications of nanocrystals that rely on ultralong WLMs.

Received 13th April 2021,
Accepted 5th July 2021

DOI: 10.1039/d1ce00488c

rsc.li/crystengcomm

Introduction

Template-assisted methods are extremely common yet highly versatile methods for preparation of nanomaterials, such as nanowires (NWs), nanorods (NRs), and nanotubes (NTs).¹ Self-assembly of surfactants may assemble various aggregate structures upon intermolecular noncovalent interactions acting as soft templates for the design of materials.² Among various types of surfactant self-assemblies, wormlike micelles (WLMs) are extremely common yet highly versatile forming above the surfactant critical micelle concentration (CMC).³ During the last few decades, WLM-based soft templates have received considerable attention.⁴ Various nanostructures, such as dendrites, NWs and NRs, have been synthesized by using cationic, anionic, zwitterionic or mixed cationic/anionic

WLM systems. The structure of WLMs can be effectively controlled by many effective approaches, such as controlling the surfactant concentration, ion concentration, pH, and temperature. Nevertheless, soft templates may lose their structural stability in the reaction process. The weak interaction between the soft template and the precursor significantly hinders structural transcription.⁵ Furthermore, ultralong NWs easily tangle and aggregate.⁶ Therefore, how to synthesize one-dimensional (1D) nanostructures with micron level length using WLM soft templates is still a great challenge.

Recent research progress in inorganic nanomaterials suggests that interfaces are the key for structure manipulation.⁷ As a result of interfacial interactions, the growth dynamics of nanocrystals can be rationally directed to desirable morphologies and/or hierarchical structures.⁸ The oil–water reaction system could provide a controlled interface for phase transfer. A three-phase fatty acid–ethanol–water system has been shown to be versatile for most monodispersed nanocrystals in the size range of 2–15 nm,⁹ including metals, metal oxides, semiconductors, organic polymers, and rare-earth fluorescent nanocrystals.¹⁰ More significantly, fatty acid-based oligomeric surfactants, such as oleic acid (OA), show novel self-assembly behaviours by electrostatic interactions with oppositely charged organic salts.¹¹

As the main inorganic phase of bones and teeth, hydroxyapatite (Ca₁₀(PO₄)₆(OH)₂, HAP) showed excellent

^a College of Chemical and Material Engineering, Quzhou University, Quzhou 324000, Zhejiang, China. E-mail: qzjht@qzc.edu.cn

^b Institute of Zhejiang University-Quzhou, Quzhou 324000, PR China

^c Zhejiang Juhua Co., Ltd., Quzhou 324004, PR China

^d Zhejiang Green Industry Development Research Institute, Quzhou 324003, PR China

^e Ningbo Institute of Materials Technology and Engineering, Chinese Academy of Sciences, Ningbo 315201, PR China

† Electronic supplementary information (ESI) available: XRD and XPS patterns of the precursors, elemental mapping and SEM-EDS images of the HAP samples, and adsorption kinetic models on hydroxyapatite/carbon. See DOI: 10.1039/d1ce00488c

usefulness as a biomaterial, adsorbent, and catalyst.¹² HAP has been considered as an environmentally benign functional material with remarkable absorbent properties.¹³ Due to the flexibility of the apatite structure, extensive substitutions are possible in all atomic sites. Furthermore, the surface electricity spot of HAP can remove pollutants by electrostatic interactions. However, it is difficult to make best use of HAP due to its hardness and brittleness.¹⁴ The toughness and strength of nanomaterials are related to the nanostructure and defects.¹⁵ 1D nanostructures, such as NWs, NRs, and NTs, have fascinated scientists because of their unique properties.¹⁶ Researchers focus their attention on how to control the morphology of HAPNWs and exploit the mechanism of the growth process by many methods, such as hydrothermal methods, homogeneous precipitation, and template methods.¹⁷

Herein, we particularly focused on the synthesis of ultralong HAPNWs in the three-phase OA-ethanol-water reaction system. HAPNWs with several tens of microscale length were prepared by formation of entangled long WLMs. A HAP/carbon composite adsorbent was also used as a potential adsorbent for the removal of methyl orange (MO) from aqueous solution. This fundamental research will enrich the knowledge base for ultralong NW design based on the WLM structure and provide insight into an effective adsorbent for the adsorption of MO from waters.

Experimental

Materials

Oleic acid (OA), sodium oleate (NaOA), calcium oleate (CaOA₂), calcium chloride (CaCl₂), sodium hydroxide (NaOH), sodium dihydrogen phosphate (NaH₂PO₄), ethanol (EtOH) and nitric acid (HNO₃) were all purchased from Sinopharm Chemical Reagent Co., Ltd., Shanghai, China. The triply distilled water was obtained using a quartz water purification system. All reagents are analytical grade and were used without further treatment.

Synthesis of ultra-long HAPNWs

To prepare the ultralong HAPNWs, an aqueous solution of CaCl₂ (0.098 M, 60 mL) was mixed with an equal volume of OA/ethanol solution (1:1, v/v) under magnetic stirring (step I). The pH value of the resulting solution was adjusted to 6.5 with a 1.25 M NaOH aqueous solution (step II). Sodium dihydrogen phosphate (0.15 M) was then slowly added to the solution under continuous magnetic stirring for 30 min, and the solution was then transferred to a Teflon-lined stainless steel autoclave, sealed, and maintained at 180 °C for 12 h (step III). This system is called HAP1#. Furthermore, an excess of 1.25 M NaOH aqueous solution was also added in step II, and an essentially stable pH value of 7.6 was reached. The same step III process above was repeated to synthesize HAP (named HAP5#).

Morphological adjustment of HAPNWs

For comparison, NaOA was dissolved in an equal volume water/ethanol solution (1:1, v/v). This solution was then mixed with an aqueous solution of CaCl₂ (0.098 M, 10 mL) under magnetic stirring, and the pH value was adjusted to 6.5 with a 0.075 M HNO₃ aqueous solution (step IV). Sodium dihydrogen phosphate was then slowly added to the solution under continuous magnetic stirring for 30 min, and the solution was transferred to a Teflon-lined stainless steel autoclave, sealed, and maintained at 180 °C for 12 h (step V). This system is called HAP2#.

CaOA₂ was dissolved in an equal volume water/ethanol solution (1:1, v/v), and the pH value was adjusted to 6.5 with a 0.075 M HNO₃ aqueous solution. After adjusting the pH value, sodium dihydrogen phosphate was slowly added to the solution under continuous magnetic stirring for 30 min, and the solution was then transferred to a Teflon-lined stainless steel autoclave, sealed, and maintained at 180 °C for 12 h (step VI). This system is called HAP3#.

Characterization of HAPNWs

Phase identification was performed by X-ray diffraction (XRD) using a Bruker AXS D8 Advance diffractometer with Cu K α radiation at a power of 1.6 kW. The surface morphology was investigated by field emission scanning electron microscopy (SEM, Hitachi S-4800, Tokyo, Japan). High-resolution transmission electron microscopy (TEM) was performed with an FEI Tecnai F20 field emission electron microscope. The rheology measurements were performed with a HAAKE rheometer (RS 6000) with a parallel plate accessory at room temperature. Oscillatory shear measurements of the samples were performed. To ensure that the storage modulus (G') and the loss modulus (G'') were independent of the applied stress, the stress amplitude was chosen in the linear viscoelastic regime as determined by dynamic stress sweep measurements.

Preparation and characterization of the composite adsorbent

The synthesis of the hydroxyapatite/carbon composite adsorbent and adsorption experiments are shown in the ESI.†

Results and discussion

Synthesis of ultralong NWs

The XRD patterns of the as-obtained samples synthesized with OA are shown in Fig. 1 (HAP1#). All of the peaks correspond to the standard diffraction pattern of Ca₅(PO₄)₃-OH (JCPDS No. 86-0740), indicating a perfect pure material with no impurities. The morphologies of the samples were investigated by TEM as shown in Fig. 1b. The HAPNWs prepared with OA formed ultralong NWs with diameters of about 25 nm, lengths of over 50 μ m and aspect ratios of above 2000. The (110) and (2 $\bar{2}$ 0) crystal planes of HAP1# were clearly revealed in the high-resolution transmission electron microscopy (HRTEM) image (Fig. 1e). In addition, the SAED

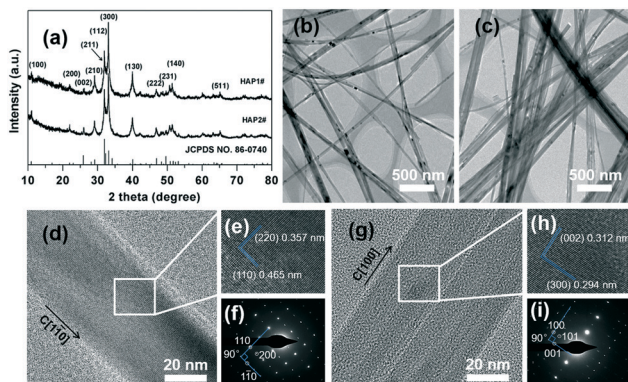


Fig. 1 Typical (a) XRD patterns; (b) TEM, (d and e) HRTEM, and (f) SAED images of the HAP1# sample; (c) TEM, (g and h) HRTEM, and (i) SAED images of the HAP2# sample.

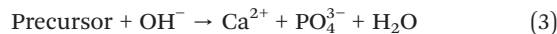
pattern (Fig. 1f) showed a set of clear single-crystal diffraction spots free of any impurities. The EDS spectrum (Fig. S1 in the ESI†) of HAP1# indicates that the Ca/P ratio is 1.71. The elemental mapping images (Fig. S1 in the ESI†) showed that the elements calcium, phosphorus, and oxygen are uniformly distributed in the structure.

In the reaction system of HAP1#, the OA-ethanol mixed liquid emulsified to form a series of waterborne microemulsions by the dropwise addition of CaCl_2 aqueous solution (step I), which is in very good agreement with the images after the emulsification process (Fig. S2 in the ESI†). With an increasing pH value from 3.0 to 6.5 using sodium hydroxide (step II), the turbid solution showed obvious viscosity enhancement from a low viscosity fluid to a highly viscoelastic fluid. The precursor used in step II of the reaction process was investigated by FT-IR spectroscopy (Fig. S3 in the ESI†). Typical $-\text{COOC}-$ symmetric stretching vibration bands are present in the $1120\text{--}1470\text{ cm}^{-1}$ region. The single peak at about 1559 cm^{-1} belonged to the asymmetric carboxylate stretching vibration of NaOA, whereas for CaOA_2 this vibration corresponds to a weak shoulder band.¹⁸ This result was in good agreement with the variation of the cation concentration in the reaction process (Fig. S4 in the ESI†). The weak signals of calcium concentration in step I could be related to the formation of microemulsions in the system with a high-organic substance content. With the increase of pH value in step II, sodium concentration was increased rapidly, and calcium concentration was sharply increased firstly and then decreased to a low concentration level. The change of the cation concentration in the system is due to the microemulsion break and phase change of oleate. This process could occur in a two-step reaction: partial dissolution of NaOA and ion exchange with Ca^{2+} , resulting in the formation of CaOA_2 :¹⁹



where R represents $-\text{CH}_3(\text{CH}_2)_7\text{CH}=\text{CH}(\text{CH}_2)_7-$.

With the addition of sodium dihydrogen phosphate (step III), the calcium phosphate ($\text{Ca}_3(\text{PO}_4)_2 \cdot x\text{H}_2\text{O}$, JCPDS No. 18-0303) precursor was formed (Fig. S5a in the ESI†), which was in good agreement with the XPS pattern (Fig. S5b in the ESI†). The HAPNWs precipitated due to the hydrolyzation process of the precursor:²⁰



Formation mechanism

For comparison and further investigation of the formation mechanism of the HAPNWs with OA, HAP was also prepared using NaOA (HAP2#) as the raw material. All the peaks in the XRD patterns of the sample correspond to the standard diffraction pattern of HAP (JCPDS No. 86-0740) as shown in Fig. 1a. This result is in very good agreement with the formation of NaOA in step II of the reaction process of HAP1#. The morphology of HAP2# was ultralong NWs similar to HAP1#.

To investigate the formation mechanism of the HAPNWs, their rheological properties in the reaction process were investigated. The experiments showed that the precursor of the HAP2# system was a highly viscoelastic fluid, which is similar to that of HAP1#. The dynamic rheological data of these two precursors exhibited a typical viscoelastic response (Fig. 2a). The storage modulus (G') crossed and prevailed over the loss modulus (G'') at high frequencies. The relaxation times of two systems are both 3.1 second. Such viscoelasticity of the solution is normally attributed to the formation of a transient network by the entanglement of long WLMs,²¹ which was confirmed by TEM investigations (Fig. 2b and c).

To reveal further the relationship between the fluid microstructure and HAP nanostructure, the characteristics of the NaOA fluid are taken into account. It is shown that the $\text{CaCl}_2/\text{NaOA}$ liquid mixture for HAP2# (step IV) is a weak alkaline medium (pH 8.5). The steady shear rheological

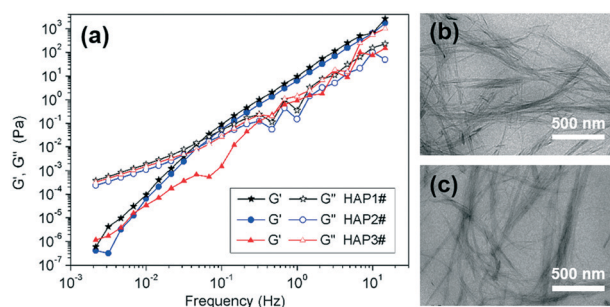


Fig. 2 (a) Storage modulus (G') and loss modulus (G'') of the precursors synthesized with different reactants. TEM images of the precursors synthesized with (b) OA and (c) NaOA.

results showed that the solution was a pseudoplastic liquid, and the viscosity of the solution increased with increasing shear rates (Fig. 3a). The rheological tests showed that this solution exhibited typical hydrogel properties in that G' was higher than G'' (Fig. 3b). The hydrogel becomes weak and softened at a decreased pH value adjusted with HNO_3 solution. The hydrogel breaks at a high shear rate in the solution at pH = 6.0 showing a property of a Newtonian fluid.

Furthermore, the solution at pH 8.5 (HAP4#) and 6.0 (HAP2#) was mixed with sodium dihydrogen phosphate (step V), respectively, and HAP was synthesized by the hydrothermal reaction. As mentioned above, HAP2# showed a similar ultralong NW morphology to HAP1#. In contrast, HAP4# has a villus morphology (Fig. S6 in the ESI†). Similar phenomena are also recorded in HAP1# with excess sodium hydroxide solution under alkaline conditions (HAP5#). The phenomenon that the structure of WLMs vary according to pH values has been reported in detail.²²

It is widely known that OA consists of a long alkyl chain and can act as a potential interfacial surfactant. In the liquid–solid–solution (LSS) strategy, OA and ethanol act as a liquid phase to control the chemical process occurring on the surface.²³ Furthermore, OA is also considered to be a structure-directing agent for efficient growth along the c axis.¹⁹ NaOA is an ultra-long-chain anionic surfactant that can dissolve in alcohol and water. The NaOA dissolved in water was partially hydrolyzed into a viscous and emulsifying liquid in both the HAP1# and HAP2# systems:



The ionized sodium ion is provided to NaOA during the pH regulation process, which compresses the electric double layers at the interface, shielding the electrostatic repulsion of OA^- molecules.²⁴ The WLM entanglement structure was then formed by reducing the distances between the charged head groups of OA^- and increasing OA^- in the micelles. It is noteworthy that the WLM structure disappeared and showed a low viscosity solution without any pH regulation. It has been reported that the WLM structure is highly responsible for the pH value.⁵ Under alkaline conditions, hydroxyl groups are normally solubilized inside the micellar cores, resulting in the disruption of the WLM structure and formation of

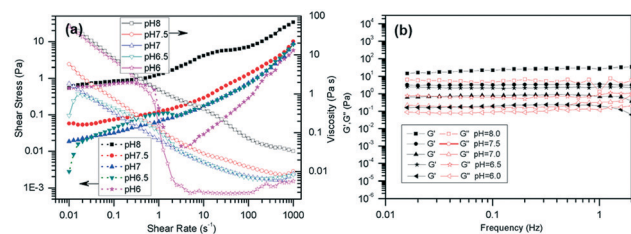


Fig. 3 (a) The steady shear rheological and (b) storage modulus (G') and loss modulus (G'') of the precursors synthesized with NaOA at different pH values in step II.

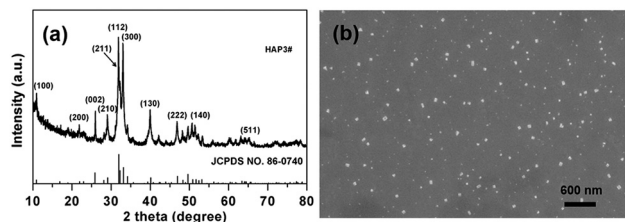


Fig. 4 Typical (a) XRD pattern and (b) SEM image of HAP3#.

spherical microemulsion droplets.²⁵ This may be the reason why this product changed to short villous structures instead of ultralong HAPNWs increasing the pH value.

Furthermore, when CaOA_2 was used as the reactant (HAP3#), the morphology of HAP3# was a square-shaped crystal with a lateral diameter of about 60 nm (Fig. 4b). The solution showed a viscous behaviour ($G' < G''$) in the whole testing frequency range (Fig. 2a), existing as parallel lines of G' and G'' at high frequency, which corresponds to the Rouse–Zimm model.²⁶ CaOA_2 is insoluble in water and soluble in ethanol. For the solution of CaOA_2 in ethanol, an oil–water interface-controlled reaction system was formed with three phases and two interfaces:⁹ CaOA_2 (solid), the ethanol–OA liquid phase (liquid) and water–ethanol solution (solution). This LSS phase transfer and separation process contributed to the formation of monodispersed nanocrystals (Fig. 4b). Therefore, the WLM structure was the key for the formation of ultralong HAPNWs.

A schematic illustration of the reaction process in the precursor and the formation of the WLM structure is shown in Fig. 5. A similar formation mechanism was reported in aqueous solution combining an anionic surfactant and inorganic salt.²¹ The main role of OA in the system is acting as a reactor and interfacial surfactant for the production of NaOA. OA is soluble in ethanol and reacts with NaOH to produce NaOA. NaOA, which is soluble in ethanol, is then hydrolyzed. Electrostatic repulsion between the OA^- head groups is shielded with increasing $[\text{Na}^+]$ and pH value from NaOH, leading to the close combination of the ionized carboxylate and NaCl, thus forming the WLM structure. OA is present as OA^- and oleate in the near-neutral solution system. Oleate shows surface activity toward the ethanol–

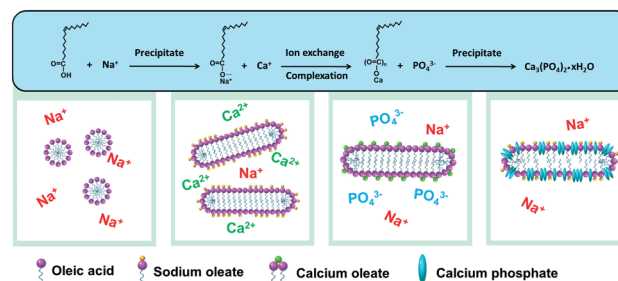


Fig. 5 Schematic illustration of the formation mechanism of the long wormlike micelles for the OA–ethanol–water reaction system.

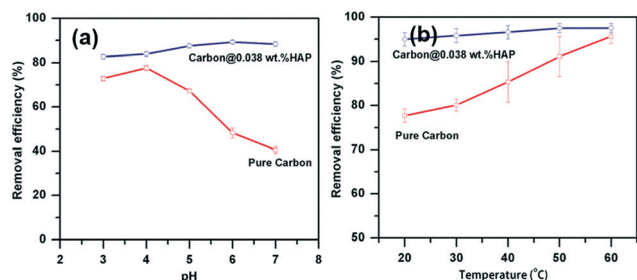


Fig. 6 Effects of (a) pH and (b) temperature on the methyl orange dye removal with pure carbon and the hydroxyapatite/carbon composite adsorbent.

water interface, which stabilizes the solution of OA^- head groups and induces the growth of the WLM structure.²⁷ CaOA_2 WLMs were further formed with the addition of Ca^{2+} ions by ion exchange with Na^+ and complexation with OA^- . The precipitation reaction between PO_4^{3-} and oleate resulted in the formation of calcium phosphate WLMs as the precursor.

Methyl orange adsorption performance evaluation

A novel composite adsorbent, hydroxyapatite/carbon (HAP1#/C), was prepared for the purpose of removing MO from aqueous solution. The impact of solution pH on the adsorption capacity over the HAP1#/C composite was examined at several pH values from 3 to 7 (Fig. 6a). The removal efficiency of the pure carbon adsorbent regularly decreased with the solution pH ranging from acid to neutral. When the pure carbon surface adsorbs excess H^+ ions in an acidic solution medium, it will show a higher adsorption capacity for negatively charged MO.²⁸ Furthermore, the adsorption process is of endothermic nature and the adsorption capacity increases with increasing temperature (Fig. 6b).^{28,29} Meanwhile, the HAP1#/C composite adsorbent showed great adsorption abilities over a broad pH and temperature range. The MO removal efficiency of HAP1#/C increased from 82.7% to 88.4% when the pH ranges from 3 to 7, and increased from 94.9% to 97.5% when the temperature increased from 20 to 60 °C.

The pseudo-first-order (PFO) and pseudo-second-order (PSO) adsorption kinetic models were utilized to evaluate the MO adsorption process (Fig. S7 in the ESI†). The linear relationships of $\log(q_e - q_t)$ vs. t and t/q_t vs. t were utilized to estimate the kinetic parameters and constants. The resulting regression coefficients (R^2) of the PSO were greater than those of the PFO, and the R^2 values of the PSO on HAP1#/C were greater than those on pure carbon.²⁹ These results showed that HAP1#/C was more conducive to chemical adsorption than pure carbon. This may be the reason why HAP1#/C showed good adsorptive abilities under broad environmental conditions. And this may be due to the functional groups Ca^{2+} , PO_4^{3-} and OH^- involved in the surface reactions,³⁰ and the removal mechanism needs further exploration.

Conclusions

Ultralong HAPNWs have been successfully fabricated in a novel three-phase OA-ethanol-water reaction system by formation of an entangled long WLM structure. The formation mechanism indicates that this type of reaction has great potential for the formation of assembled nanocrystals using ultralong WLMs. This fundamental research is important for controlled synthesis and applications of stimuli-responsive WLMs.

Conflicts of interest

The authors declare that there is no conflict of interest regarding the publication of this article.

Acknowledgements

This research was funded by the Scientific Research Fund of Zhejiang Provincial Education Department (No. Y201533679), the Personnel Training Foundation of Quzhou University (No. BSYJ201412), the Young and Middle-aged Academic Backbone Training Project (special funds of the construction of teachers' team of Quzhou University) (No. XNZQN201507), and the College Students' National Innovation and Entrepreneurship Projects (Nos. 201711488009, 201811488016, and 202011488001).

Notes and references

- (a) B. S. Chen, Q. L. Xu, X. L. Zhao, X. G. Zhu, M. G. Kong and G. W. Meng, *Adv. Funct. Mater.*, 2010, **20**, 3791; (b) X. L. Niu, K. D. Lv, E. G. Liu, S. B. Zhu and W. Z. Zhang, *J. Mol. Liq.*, 2021, **322**, 114974.
- (a) E. N. Zare, M. M. Lakouraj and A. Achna, *J. Mol. Liq.*, 2018, **271**, 514; (b) W. Jin, R. R. Wang and X. R. Huang, *J. Mol. Liq.*, 2020, **312**, 113442.
- (a) Y. J. Song, R. M. Garcia, R. M. Dorin, H. R. Wang, Y. Qiu and G. N. Coker, *Nano Lett.*, 2007, **12**, 3650; (b) Y. Zhang, N. Y. Nishi, K. I. Amano and T. Sakka, *Electrochim. Acta*, 2018, **282**, 886.
- (a) A. D. Wang, W. Y. Shi, J. B. Huang and Y. Yan, *Soft Matter*, 2016, **12**, 337; (b) T. T. Yan, B. L. Song, D. L. Du, Z. G. Cui and X. M. Pei, *J. Colloid Interface Sci.*, 2020, **579**, 61; (c) B. Li, N. You, Y. C. Liang, Q. Zhang, W. J. Zhang, M. Chen and X. C. Pang, *Energy Environ. Mater.*, 2019, **2**, 38.
- (a) X. P. Gao, F. Lu, B. Dong, Y. Z. Liu, Y. N. Gao and L. Q. Zheng, *Chem. Commun.*, 2015, **51**, 843; (b) X. P. Gao, F. Lu, W. J. Yang, F. K. Shang and L. Q. Zheng, *RSC Adv.*, 2016, **6**, 67495.
- F. Chen and Y. J. Zhu, *ACS Nano*, 2016, **10**, 11483.
- (a) H. Y. Shi, B. Hu, X. C. Yu, T. L. Zhao, X. F. Ren, S. L. Liu, J. W. Liu, M. A. Feng, W. Xu and S. H. Yu, *Adv. Funct. Mater.*, 2010, **20**, 958; (b) X. D. Wang, Z. D. Li, J. Shi and Y. H. Yu, *Chem. Rev.*, 2014, **114**, 9346; (c) J. C. Liu, H. W. Bai, Y. J. Wang, Z. Y. Liu, X. W. Zhang and D. D. Sun, *Adv. Funct. Mater.*, 2010, **20**, 4175.

- 8 (a) Z. Qin and M. J. Buehler, *Nanotechnology*, 2018, **29**, 280201; (b) Y. Zhao, J. D. Chen, L. Zou, G. Xu and Y. S. Geng, *Chem. Eng. J.*, 2019, **378**, 122174; (c) J. Ren, Y. W. Liu, D. L. Kaplan and S. J. Ling, *MRS Bull.*, 2019, **44**, 53.
- 9 (a) J. F. Hui and X. Wang, *Chem. – Eur. J.*, 2011, **17**, 6926; (b) X. Wang, J. Zhuang, Q. Peng and Y. D. Li, *Adv. Mater.*, 2006, **18**, 2031; (c) H. P. Yu, Y. J. Zhu and B. Q. Lu, *Ceram. Int.*, 2018, **44**, 12352; (d) Z. C. Xiong, Y. J. Zhu, F. F. Chen, T. E. Sun and Y. Q. Shen, *Chem. – Eur. J.*, 2016, **22**, 11224; (e) Z. C. Xiong, R. L. Yang, Y. J. Zhu, F. F. Chen and L. Y. Dong, *J. Mater. Chem. A*, 2017, **5**, 17482.
- 10 (a) X. Wang, J. Zhuang, Q. Peng and Y. D. Li, *Nature*, 2005, **437**, 121; (b) X. Wang, Q. Peng and Y. D. Li, *Acc. Chem. Res.*, 2007, **40**, 635.
- 11 C. W. Li, D. H. Xie, X. M. Pei, B. L. Song and Z. G. Cui, *Colloid Polym. Sci.*, 2019, **297**, 125.
- 12 (a) Y. L. Li, H. Y. Zhou, G. X. Zhu, C. Y. Shao, H. H. Pan, X. R. Xu and R. K. Tang, *J. Hazard. Mater.*, 2015, **299**, 379; (b) K. Mori, T. Hara, T. Mizugaki, K. Ebitani and K. Kaneda, *J. Am. Chem. Soc.*, 2004, **126**, 10657.
- 13 (a) N. C. Zheng, L. Y. Yin, M. H. Su, Z. Q. Liu and D. C. W. Tsang, *Chem. Eng. J.*, 2020, **384**, 123262; (b) L. J. Dong, Z. L. Zhu, Y. L. Qiu and J. F. Zhao, *Chem. Eng. J.*, 2010, **165**, 827; (c) P. Karthikeyan, S. S. D. Elanchezhyan, H. A. T. Banu, M. H. Farzana and C. M. Park, *Chemosphere*, 2021, **276**, 130200.
- 14 L. Ma, T. Y. Hao and Z. M. Hossain, *J. Appl. Phys.*, 2019, **126**, 164303.
- 15 S. Pai, M. S. Kini and R. Selvaraj, *Environ. Sci. Pollut. Res.*, 2021, **28**, 11835.
- 16 (a) J. F. Hui and X. Wang, *Inorg. Chem. Front.*, 2014, **1**, 215; (b) Z. J. Liu, L. Chen, Z. C. Zhang, Y. Y. Li, Y. H. Dong and Y. B. Sun, *J. Mol. Liq.*, 2013, **179**, 46; (c) A. Haider, S. Haider, S. S. Han and I. K. Kang, *RSC Adv.*, 2017, **7**, 7442.
- 17 (a) B. Song, Y. L. Zhong, S. Wu, B. B. Chu, Y. Y. Su and Y. He, *J. Am. Chem. Soc.*, 2016, **138**, 4824; (b) J. Tian, Z. H. Zhao, A. Kumar, R. I. Boughton and H. Liu, *Chem. Soc. Rev.*, 2014, **43**, 6920; (c) Y. Liu, W. Y. Zhen, Y. H. Wang, J. H. Liu, L. H. Jin, T. Q. Zhang, S. T. Zhang, Y. Zhao, S. Y. Song, C. Y. Li, J. J. Zhu, Y. Yang and H. J. Zhang, *Angew. Chem., Int. Ed.*, 2019, **58**, 2407.
- 18 X. Y. Zheng, M. Y. Liu, J. F. Hui, D. D. Fan, H. X. Ma, X. Y. Zhang, Y. Y. Wang and Y. Wei, *Phys. Chem. Chem. Phys.*, 2015, **17**, 20301.
- 19 (a) M. L. Qi, J. Qi, G. Y. Xiao, K. Y. Zhang, C. Y. Lu and Y. P. Lu, *CrystEngComm*, 2016, **18**, 5876; (b) X. Liu, K. X. Li, C. Q. Wu, Z. Q. Li, B. Wu, X. H. Duan, Y. Zhou and C. H. Pei, *CrystEngComm*, 2019, **21**, 4859.
- 20 (a) J. Kou, D. Tao, T. Sun and G. Xu, *Trans. Soc. Min., Metall., Explor.*, 2012, **29**, 47; (b) C. Liu, Q. M. Feng and G. F. Zhang, *Miner. Eng.*, 2015, **84**, 74; (c) W. Q. Gong, A. Parentich, L. H. Little and L. J. Warren, *Langmuir*, 1992, **8**, 118.
- 21 (a) F. F. Chen, Z. Y. Yang, Y. J. Zhu, Z. C. Xiong, L. Y. Dong, B. Q. Lu, J. Wu and R. L. Yang, *Chem. – Eur. J.*, 2018, **24**, 416; (b) Y. Y. Jiang, Y. J. Zhu, F. Chen and J. Wu, *Ceram. Int.*, 2015, **41**, 6098.
- 22 (a) X. J. Ye, C. C. Zhou, Z. W. Xiao, Y. J. Fan, X. D. Zhu, Y. Sun and X. D. Zhang, *Mater. Lett.*, 2014, **128**, 179; (b) W. W. Chu, Z. Z. Lu, R. Q. Tan, S. H. Tang, W. Xu, W. J. Song and J. H. Zhao, *Powder Technol.*, 2018, **329**, 420.
- 23 (a) W. L. Kang, T. Y. Zhu, P. X. Wang, X. Y. Hou, Y. L. Zhao, X. F. Zhang and H. B. Yang, *J. Mol. Liq.*, 2019, **286**, 110946; (b) B. G. Wang, L. Liu, C. C. Zheng and H. S. Lu, *J. Dispersion Sci. Technol.*, 2018, **39**, 539.
- 24 (a) Z. H. Yan, H. N. Sun, Z. H. Ni, X. Lu, H. B. Lv and M. Li, *J. Mol. Liq.*, 2019, **278**, 195; (b) P. X. Wang, T. Y. Zhu, X. Y. Hou, Y. L. Zhao, X. F. Zhang, T. Y. Wang, H. B. Yang and W. L. Kang, *J. Mol. Liq.*, 2019, **286**, 110935; (c) W. L. Kang, T. Y. Zhu, P. X. Wang, X. Y. Hou, Y. L. Zhao, X. F. Zhang and H. B. Yang, *J. Mol. Liq.*, 2019, **286**, 110946.
- 25 (a) L. L. Liu, J. P. Huang, Y. M. Feng, J. Liu and X. B. Yu, *Adv. Powder Technol.*, 2015, **26**, 428; (b) J. P. Sun, X. Y. Zheng, H. Li, D. D. Fan, Z. P. Song, H. X. Ma, X. F. Hua and J. F. Hui, *Mater. Sci. Eng., C*, 2017, **73**, 596.
- 26 H. S. Lu, Q. P. Shi and Z. Y. Huang, *J. Phys. Chem. B*, 2014, **118**, 12511.
- 27 C. L. Chen, S. S. Wang, B. P. Grady, J. H. Harwell and B. J. Shiao, *Langmuir*, 2019, **35**, 12168.
- 28 (a) B. Acemioglu, *Int. J. Coal Prep. Util.*, 2019, **39**, 1; (b) M. H. Bilir, N. Sakalar, B. Acemioglu, E. Baran and M. H. Alma, *J. Appl. Polym. Sci.*, 2013, **127**(6), 4340.
- 29 D. Robati, B. Mirza, M. Rajabi, O. Moradi, I. Tyagi, S. Agarwal and V. K. Gupta, *Chem. Eng. J.*, 2016, **284**, 687.
- 30 (a) S. Hokkanen, A. Bhatnagar, E. Repo, S. Lou and M. Sillanpaa, *Chem. Eng. J.*, 2016, **283**, 445; (b) W. Zheng, X. M. Li, Q. Yang, G. M. Zeng, X. X. Shen, Y. Zhang and J. J. Liu, *J. Hazard. Mater.*, 2007, **147**, 534.